⌘ *Author's Choice*

THE JOURNAL OF BIOLOGICAL CHEMISTRY VOL. 285, NO. 53, pp. 41765–41771, December 31, 2010

Imaging of Mobile Long-lived Nanoplatforms in the Live Cell Plasma Membrane*[S]

Received for publication, September 4, 2010, and in revised form, October 18, 2010 Published, JBC Papers in Press, October 21, 2010, DOI 10.1074/jbc.M110.182121

Mario Brameshuber[‡], Julian Weghuber[‡], Verena Ruprecht[‡], Imre Gombos[§], Ibolya Horváth[§], László Vigh[§], Paul Eckerstorfer[¶], Endre Kiss[¶], Hannes Stockinger[¶], and Gerhard J. Schütz[‡1]

From the [‡]Biophysics Institute, Johannes Kepler University Linz, Altenbergerstrasse 69, A-4040 Linz, Austria, the [§]Institute of Biochemistry, Biological Research Center, Hungarian Academy of Sciences, H-6701 Szeged, Hungary, and the [¶]Department of Molecular Immunology, Center for Pathophysiology, Infectiology, and Immunology, Medical University of Vienna, Lazarettgasse 19, A-1090 Vienna, Austria

The plasma membrane has been hypothesized to contain nanoscopic lipid platforms, which are discussed in the context of "lipid rafts" or "membrane rafts." Based on biochemical and cell biological studies, rafts are believed to play a crucial role in many signaling processes. However, there is currently not much information on their size, shape, stability, surface density, composition, and heterogeneity. We present here a method that allows for the first time the direct imaging of nanoscopic long-lived platforms with raft-like properties diffusing in the live cell plasma membrane. Our method senses these platforms by their property to assemble a characteristic set of fluorescent marker proteins or lipids on a time scale of seconds. A special photobleaching protocol was used to reduce the surface density of labeled mobile platforms down to the level of well isolated diffraction-limited spots without altering the single spot brightness. The statistical distribution of probe molecules per platform was determined by single molecule brightness analysis. For demonstration, we used the consensus raft marker glycosylphosphatidylinositol-anchored monomeric GFP and the fluorescent lipid analog BODIPY-G_{M1}, which preferentially partitions into liquid-ordered phases. For both markers, we found cholesterol-dependent homo-association in the plasma membrane of living CHO and Jurkat T cells in the resting state, thereby demonstrating the existence of small, mobile, long-lived platforms containing these probes. We further applied the technology to address structural changes in the plasma membrane during fever-type heat shock: at elevated temperatures, the glycosylphosphatidylinositol-anchored monomeric GFP homo-association disappeared, accompanied by an increase in the expression of the small heat shock protein Hsp27.

The organization of the cell plasma membrane at a nanoscopic length scale is believed to affect the association of distinct sets of membrane proteins for the regulation of various signaling pathways (1, 2). Conflicting models have been proposed that postulate the existence of long-lived (3) or short-lived (4, 5) platforms of membrane lipids and proteins, commonly termed lipid or membrane rafts. In the beginning, rafts were proposed as the physical representation of plasma membrane fractions that were found to be resistant to treatment with mild non-ionic detergents (3, 6). Based on comparative analysis of detergent-soluble and detergent-insoluble membrane fractions, rafts were described to recruit particularly proteins with hydrophobic modifications such as a glycosylphosphatidylinositol (GPI)[2] anchor, a double acylation, or a palmitoyl group (6–10). Lipids enriched in the detergent-resistant or detergent-soluble membrane fraction were found to form a liquid-ordered or liquid-disordered phase (11), respectively, which is frequently taken as an indication that phase separation may drive the formation of rafts. However, a note of caution was raised against the structural interpretation of biochemical data by pointing out that rafts may be altered or even formed upon detergent treatment (12).

The small size and high surface density of membrane rafts impair straightforward light microscopy approaches; indeed, homogenous surface distribution has been reported for many putative raft markers (13). Therefore, only few studies addressed the nanoscopic organization directly in the live cell plasma membrane. For example, based on the concentration dependence of the homo-FRET between GPI-anchored proteins, researchers concluded the association of these proteins to nanometer-sized domains (14–16). Moreover, a clever variant of fluorescence correlation spectroscopy was recently introduced to study subtle heterogeneities in the surface distribution of fluorescent lipid analogs and GPI-anchored proteins (17, 18). The interpretation of both results depends strongly, however, on presumed raft properties, rendering an *a priori* proof and further characterization difficult. In consequence, the methodological deficit, together with oversimplified models, yielded skepticism even in the existence of such nanostructures (19, 20).

In summary, we currently face a spectrum of supposed raft characteristics that give rise to an all-in-one terminology suit-

* This work was supported by Austrian Science Fund Projects Y250-B03 and I301-B12, the GEN-AU Project of the Austrian Federal Ministry for Science and Research and the European Union Project LipidomicNet (HEALTH-F4-2008-202272), and Hungarian National Scientific Research Foundation Grants NK 68379 and NN 76716.

⌘ *Author's Choice*—Final version full access.

[S] The on-line version of this article (available at http://www.jbc.org) contains supplemental "Materials and Methods," "Discussion," Figs. 1–7, Tables 1 and 2, Equation S1, and additional references.

[1] To whom correspondence should be addressed. Tel.: 43-732-2468-9284; Fax: 43-732-2468-29284; E-mail: gerhard.schuetz@jku.at.

[2] The abbreviations used are: GPI, glycosylphosphatidylinositol; mGFP, monomeric GFP; HBSS, Hanks' buffered salt solution; MβCD, methyl-β-cyclodextrin; TOCCSL, thinning out clusters while conserving stoichiometry of labeling.

able for a multitude of purposes. We wanted to address a specific aspect originally ascribed to rafts: the property to stably assemble a characteristic set of proteins and lipids within nanoscopic mobile domains (3). For this, we developed a new single molecule imaging modality that allows for detecting and quantifying the homo-association of mobile membrane constituents at high surface density (21, 22). We use the term homo-association to indicate any long-lived colocalization of multiple copies of a specific probe. Here, we provide evidence that a GPI-anchored monomeric GFP (mGFP-GPI) as a consensus raft marker (8, 14) and the fluorescent lipid analog BODIPY-G_{M1} as liquid-ordered phase marker (23) indeed diffuse as integral parts of long-lived nanoscopic platforms in the live cell plasma membrane. We show that the integrity of the platforms depends on cholesterol, indicating a relation to biochemically defined rafts.

MATERIALS AND METHODS

Fusion Constructs and Cell Culture—The GFP-GPI plasmid (a kind gift from Jennifer Lippincott-Schwartz, National Institutes of Health, Bethesda, MD) was constructed from the GPI signal sequence of the human folate receptor in the eukaryotic expression vector pJB20. Details on the construct and the cell cultures used are provided under supplemental "Materials and Methods."

Characterization of the Detergent Resistance of mGFP-GPI—Detergent-resistant microdomain separation was performed for CHO cells via sucrose gradient centrifugation (24) and for Jurkat T cells using the flow cytometric assay of detergent resistance (25). Detailed descriptions are provided under supplemental "Materials and Methods."

Sample Preparation—CHO cells were washed two times with a 37 °C Hanks' buffered salt solution (HBSS; PAA Laboratories) and mounted in a POCmini chamber system (LaCon, Staig, Germany) filled with HBSS. BODIPY FL C_5-ganglioside G_{M1} (B-13950, Invitrogen) was diluted in HBSS and used to label CHO cells at various concentrations ranging from 50 to 500 nM at 4 °C for 20 min on ice. Additional washing steps were applied to remove unbound BODIPY-G_{M1}.

Labeling of Jurkat cells was performed as described previously (26) and under supplemental "Materials and Methods." For cholesterol depletion experiments, cells were washed twice with HBSS and incubated with 10 mM methyl-β-cyclodextrin (MβCD; C4555, Sigma) at 37 °C for 20 min. Cholesterol oxidase (C8649, Sigma) was applied at 37 °C for 30 min at 2 units/ml (CHO cells) or at 10 units/ml (Jurkat T cells). For BODIPY-G_{M1} experiments, cholesterol depletion was performed before staining. The extent of cholesterol depletion was determined using the Amplex Red cholesterol assay kit (A12216, Invitrogen).

For cholesterol replenishment experiments, cells were first depleted using MβCD via the above protocol. Cholesterol (700000P, Avanti Polar Lipids, Alabaster, AL) was replenished by incubation with 10 mM cholesterol-loaded MβCD for 30 min at 37 °C in HBSS following the protocol of Yancey *et al.* (27). For experiments with BODIPY-G_{M1}, cells were first replenished with cholesterol and subsequently labeled with the lipid analog.

For cleavage of GPI-anchored proteins, we incubated mGFP-GPI-expressing CHO cells for 3 h with 0.5 units/ml phosphatidylinositol-specific phospholipase C (P5542, Sigma) in HBSS at 37 °C. Trypan blue (33595, Sigma) was added at 0.4% in HBSS at 37 °C and measured immediately.

Supported Lipid Bilayer Preparation—Purified His-mGFP-GPI(CD55) was a kind gift from Christoph Metzner (Institute for Virology, University of Veterinary Medicine Vienna, Wien, Austria). The protein was purified as described (28), except for using a HEK293 cell line as the expression system. Supported lipid bilayers were formed from vesicles as described under supplemental "Materials and Methods" (29).

Western Blotting—mGFP-GPI-expressing CHO cells at 60–70% confluency were subjected to heat at the indicated temperatures (±0.1 °C) in a water bath for 1 h. After a 20-h incubation at 37 °C in a 5% CO_2 atmosphere, cells were washed with PBS and lysed with Laemmli sample buffer. Western blotting was performed as described under supplemental "Materials and Methods."

Microscopy—Single molecule experiments were performed on a setup described in detail under supplemental "Materials and Methods" (21). Temperature was controlled using a home-built incubator box equipped with a heating unit, a temperable stage insert, and an objective heater (PeCon, Erbach, Germany). For heat shock experiments, cells were grown at 37 °C and adjusted to the indicated temperature immediately before the experiments.

After recording a pre-bleach image with an illumination time of 1 ms, samples were bleached with a laser pulse applied for 200–450 ms. After a variable recovery time of 600–2400 ms, a sequence of up to 10 images was recorded at an illumination time of 1 ms with a typical delay of 20 ms between subsequent images. The first image after bleaching was used for brightness analysis and the consecutive images for determination of mobilities. Because of the small bleaching area, multiple runs could be performed on a single cell without significant reduction of the total amount of active fluorophores on this cell.

The single molecule brightness was obtained after multiple runs of thinning out clusters while conserving the stoichiometry of labeling (TOCCSL) by extensively photobleaching the same cell for seconds. In this case, the probability for observing more than one active mGFP-GPI molecule per spot became negligible. Alternatively, we used the brightness values obtained in the last image of a sequence, which, due to photobleaching, contained a reduced number of peaks; also in this case, the likelihood that two molecules of dimer remained active was negligible (supplemental Fig. 3*A*). Both methods yielded the same results.

For the precise control of all laser pulse trains, an acousto-optical modulator (1205C, Isomet, Springfield, VA) was used. Timing protocols were generated and controlled by an in-house program package implemented in LABVIEW (National Instruments, Austin, TX).

Data Analysis—For single molecule analysis, images were analyzed using in-house algorithms implemented in MATLAB (MathWorks, Natick, MA) (30). Individual diffraction-limited signals were selected and fitted with a Gaussian pro-

file, yielding the single molecule position, the brightness (B), and the full width at half-maximum of the Gaussian function. Single molecule mobility and brightness were analyzed as described under supplemental "Materials and Methods" and in Refs. 21, 30, and 31.

The surface density of BODIPY-G_{M1} was determined by dividing the pre-bleach signal by the average single molecule brightness ($\rho_1(B)$). α-Distributions were fitted with a generalized Poisson model that accounts also for observation of non-raft resident free probes (Equation 1).

$$\alpha_n = (1 - P)\frac{\lambda^n \exp(-\lambda)}{n!} + P(1 - H(n - 1)) \qquad \text{(Eq. 1)}$$

In this model, λ specifies the expectation value of the Poisson distribution, P the probe partitioning into the non-raft phase, and H the unit step function. Mobile fractions were measured via standard fluorescence recovery after photobleaching experiments: the equilibrium ensemble signal obtained after photobleaching was normalized by the pre-bleach signal.

RESULTS

Experimental Strategy—We generated a CHO cell line stably expressing the consensus raft marker mGFP-GPI (8, 14, 32). Using sucrose density gradient centrifugation or a flow cytometric assay of detergent resistance (25), we found similar mGFP-GPI partitioning into the raft phase as reported previously (compare supplemental Fig. 1 and Ref. 32). The probe was specifically targeted to the plasma membrane, yielding the expected homogenous staining without enrichment in resolvable microdomains (Fig. 1, *A* and *B*). We were interested in whether the apparent homogenous signal was caused by hundreds of mobile nanoscopic platforms per diffraction-limited area. In our approach, we aimed at detecting such platforms via their property to assemble specific markers over time scales of seconds. It was therefore necessary to populate each platform with multiple markers, so we selected for cell lines with high mGFP-GPI surface staining. To virtually dilute stable mobile fluorescent assemblies without altering their properties, we made use of a recently introduced photobleaching protocol (TOCCSL) (21).

Fig. 1 (*B–D*) illustrates the method: the *upper panels* show the sample during the TOCCSL sequence, and the *lower panels* sketch the effect on putative membrane platforms. After recording an image of the undisturbed plasma membrane (Fig. 1*B*), a narrow stripe is irreversibly photobleached (Fig. 1*C*). High contrast in photobleaching is achieved by imaging a field stop onto the sample, which ensures minimal photobleaching of structures located outside the illuminated region; we used here a slit aperture with a width of 7 μm in the specimen plane. Diffusional broadening is minimized by applying short photobleaching times and high laser power. Brownian motion of the platforms leads to the recovery of the fluorescence signal (33). At the onset of this process, the first platforms diffusing into the field of view can be imaged directly as individual isolated fluorescent spots (Fig. 1*D*). To minimize contributions from the cytosol or the top cell membrane, we performed all experiments in total internal reflection configuration at the glass slide/cell interface. Fig. 1*D* further shows that the recovery proceeds from the masked region, with the central region of the field of view being devoid of signals. This observation confirms that the detected signals correspond to plasma membrane-associated mGFP-GPI; a potential vesicular pool would have traversed the evanescent field directly from the top, thereby repopulating the photobleached area uniformly over the field of view (see also supplemental "Discussion," Subsection 1, for further controls).

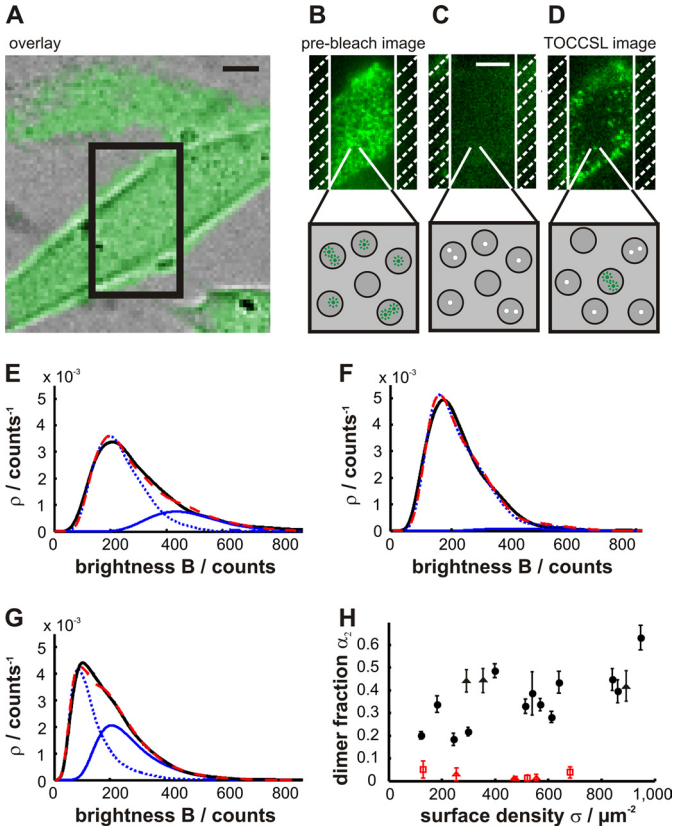

FIGURE 1. **Observation of mGFP-GPI clusters in the plasma membrane of living CHO cells.** The principle of the TOCCSL method is shown in *A–D*. *A*, overlay of a white light image and the fluorescent image of a mGFP-GPI-expressing CHO cell. The *box* indicates the region of interest chosen for the TOCCSL sequence. *B–D*, different steps of the illumination protocol. The *upper panels* present the original data; the *lower panels* present a sketch of the effect on putative membrane platforms. Active and photobleached fluorophores are indicated by *green* and *white dots*, respectively. The *white hatched areas* indicate the position of the field stop (width of 7 μm). After recording the pre-bleach image (*B*), the selected area was totally photobleached by a laser pulse (450 ms). The efficiency of photobleaching was controlled by an image recorded immediately after the bleach pulse (recovery time of 0.5 ms). After a recovery time of 800 ms, the first fluorescent spots entering the field of view could be observed as diffraction-limited signals. For display, the color axis range was reduced by a factor of 5 in *C* and *D*. The brightness distributions of single mGFP-GPI spots in CHO cells without (*E*) and after cholesterol depletion with MβCD (*F*) are plotted as probability density functions. *G*, data obtained after cholesterol depletion and subsequent replenishment with MβCD. Data (*black line*) were fitted by Equation S1 (*red line*); monomer (*dotted line*) and dimer (*solid line*) contributions are indicated in *blue*. *H*, the dimer fraction (α_2) as a function of mGFP-GPI surface density (σ). Each data point resulted from the analysis of a single cell on which multiple TOCCSL runs were performed. Experiments are shown under standard conditions (*black circles*) or after cholesterol depletion using MβCD (*red triangles*) or cholesterol oxidase (*red squares*). Data obtained after cholesterol depletion and subsequent replenishment with MβCD are indicated as *black triangles*. σ was obtained from the pre-bleach image by dividing the overall signal by the single molecule brightness. All experiments were performed at 37 °C. *Scale bars* = 5 μm.

Cholesterol-dependent mGFP-GPI Homo-association—We studied the mGFP-GPI association state by analyzing the brightness of individual fluorescent spots observed in the TOCCSL images (Fig. 1*D*). A broad distribution of brightness values (B) was obtained as expected from the stochastic nature of the photon emission process (Fig. 1*E*; see supplemental Table 2 for information on sample sizes). For comparison, we also plotted the brightness distribution of single mGFP-GPI molecules, which was determined from the same experiments upon additional photobleaching (see *Microscopy* under "Materials and Methods" and supplemental Fig. 3*A*). Single molecule signals showed a substantially reduced brightness compared with spots obtained in the TOCCSL images, indicating that the latter represent a mixed population of mGFP-GPI monomers and homo-associates.

For quantification of the association state of mGFP-GPI, we fitted $\rho(B)$, the brightness distribution obtained in the TOCCSL images, by a linear combination of the n-mer brightness distributions ($\rho_n(B)$); the weights (α_n) specify the fraction of n-mers (see *Data Analysis* under "Materials and Methods"). The majority of spots were found to correspond to mGFP-GPI monomers ($\alpha_1 = 67.8 \pm 0.8\%$) (Fig. 1*E*). Importantly, $\alpha_2 = 32.3 \pm 0.8\%$ of the spots contained two mGFP-GPI molecules, indicating the presence of stable homo-association of GPI-anchored proteins in this system. Coefficients ($\alpha_{n>2}$) representing three or more molecules per spot did not yield detectable contributions here.

Cholesterol has been ascribed an essential role for the targeting of GPI-anchored proteins to membrane rafts (1, 14, 17). We therefore tested whether cholesterol depletion affects the observed mGFP-GPI homo-association. Indeed, a reduction of the cellular cholesterol content by 30% using either MβCD or cholesterol oxidase fully abolished mGFP-GPI homo-association (Fig. 1, *F* and H), consistent with the interpretation that the platforms were disrupted or the partitioning to the platforms was abolished. The effect was reversible, as cholesterol replenishment recovered the dimer fraction essentially to the level of the untreated control samples (Fig. 1*G*). In further controls, we ruled out that laser excitation (supplemental Fig. 3*B*) or GFP self-association could account for the observed results (see supplemental "Discussion," Subsection 2).

We next addressed the dependence of α_2 on the surface density of mGFP-GPI (σ). It was reported previously using standard wide-field microscopy that the degree of protein nanoclustering did not depend on the average cell brightness (14, 15). We attempted to obtain a more accurate measure for σ by using the total internal reflection fluorescence prebleach image from each cell. A high cell-to-cell variability of both α_2 and σ was found (Fig. 1*H*), and interestingly, we observed a small but clear increase in α_2 with σ. Apparently, cells expressing higher amounts of mGFP-GPI in their plasma membrane also show a higher cargo load per platform.

Dynamic Characterization of the Observed Structures—In recent years, there was an opinion shift under raft proponents from long- toward short-lived rafts, with lifetimes speculated in the submillisecond range (4, 5). We therefore used our method to address the cargo exchange dynamics between different platforms. All fluorescent structures observed in the TOCCSL image had multiple encounters with photobleached structures during the recovery time, with multiple chances for cargo exchange. In particular, subsecond disintegration and reformation of structures hosting non-bleached mGFP-GPI would lead to cargo equilibration with photobleached platforms. The result would be a decrease in the single spot brightness (B) and concomitantly the dimer weight (α_2) with increasing recovery times. However, we found no dependence of α_2 on the recovery time (correlation coefficient = 0.037) (supplemental Fig. 5*A*). We conclude that the lifetime of the observed platforms substantially exceeds the maximum recovery time used in our experiments of 2.2 s.

We next questioned whether the loading of the observed structures correlates with their size. In particular, we were interested in whether the observed mGFP-GPI monomers resided in similar platforms as clusters of higher order or represented a population leaking into the non-raft bulk phase. The mobility of a diffusing tracer in a lipid membrane decreases with increasing size (34, 35), rendering the diffusion constant (D) a valid measure for the size of the moving structure. On average, the motion of mGFP-GPI was characterized by $D = 1.30 \pm 0.08\ \mu m^2/s$ (supplemental Fig. 6*A*), in agreement with the recent literature (17). We detected no difference in the mobility of the mGFP-GPI species observed in the TOCCSL images *versus* results obtained on single molecule data recorded after extensive photobleaching of the cells ($D = 1.20 \pm 0.17\ \mu m^2/s$) (supplemental Fig. 6*B*), indicating that the molecules observed in the TOCCSL images are representative for the mobile fraction of plasma membrane-associated mGFP-GPI (76 ± 5%) (supplemental Table 1). Consistent with recent literature (36, 37), the mobility of mGFP-GPI decreased substantially upon cholesterol depletion (supplemental Fig. 6*C*). To check for different populations of mGFP-GPI, we compared the brightness with the mobility of each diffusing spot (supplemental Fig. 5*B*; see supplemental Fig. 7*A* for the correlation plot on cholesterol-depleted cells). We found hardly any correlation between the two parameters (correlation coefficients of −0.085 and −0.089 for untreated and cholesterol-depleted cells, respectively), indicating that the observed spots are similar in mobility and therefore in size, irrespective of whether they are loaded with one or two mGFP-GPI molecules. Our finding is thus consistent with the interpretation that all observed signals correspond to similar platforms.

External Loading with BODIPY-G_{M1}—Having shown the homo-association of an ectopically expressed protein, we next attempted to confirm the results using an externally applied probe. We used BODIPY-G_{M1}, a fluorescent lipid analog that was reported recently to be enriched in the liquid-ordered phase of plasma membrane vesicles (23). When applied to CHO cells, we found that BODIPY-G_{M1} homo-associated in a cholesterol-dependent manner (Fig. 2*A*). We measured the association at different probe densities in the plasma membrane: at a surface density (σ) of 2600 μm^{-2}, we determined $\alpha_2 = 0.26 \pm 0.02$, which decreased linearly with decreasing probe densities. The linear dependence of homo-association on surface density is plausible for the externally applied

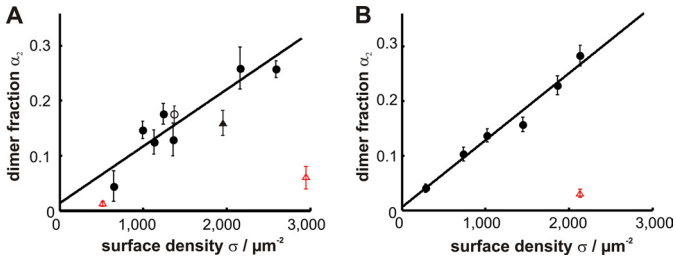

FIGURE 2. **Dimer fraction of the externally applied probe BODIPY-G_{M1}.** Cells were stained with BODIPY-G_{M1}, and the dimer fraction (α_2) was determined for different surface densities (σ). We found a linear increase in α_2 with σ in CHO cells (*A*, *black circles*) and Jurkat T cells (*B*, *black circles*). Upon cholesterol depletion using MβCD, the dimer fraction was dramatically reduced (*red triangles*). Cholesterol replenishment recovered the original dimer fraction (*black triangle*). We included one experiment in which BODIPY-G_{M1} labeling was performed at 37 °C (*white circle*), indicating that the labeling temperature of 4 °C used in all other experiments had no influence on the observed association. Microscopy was performed at 37 °C.

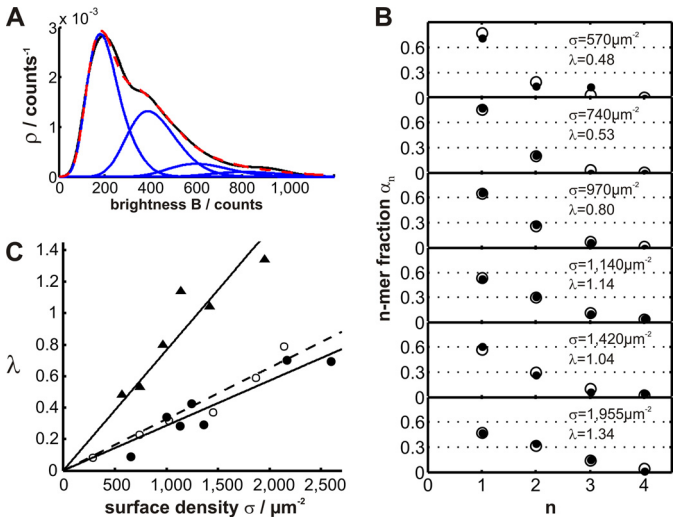

FIGURE 3. **Stoichiometric composition of BODIPY-G_{M1} clusters.** TOCCSL experiments were performed on Jurkat T cells at 25 °C using BODIPY-G_{M1} as the label. Brightness distributions were analyzed for various stainings, with *A* providing a showcase for $\sigma = 1140\ \mu m^{-2}$; the display is analogous to Fig. 1*E*. In this case, higher order cluster sizes up to tetramers were observed and included in the fit function. *B*, relative amount of cluster size *n* (α_n) obtained for five different surface densities (σ; *black circles*). Fit results based on a generalized Poisson model (Equation 1) are shown as *white circles*. *C*, the fit parameter (λ) is plotted as a function of the surface density (σ; *triangles*). Linear fitting yielded a slope (ζ) of 1300 platforms/μm^2. For comparison, we also included λ calculated for CHO cells at 37 °C (*black circles*; $\zeta = 3500\ \mu m^{-2}$) and Jurkat T cells at 37 °C (*white circles*; $\zeta = 3100\ \mu m^{-2}$). This experiment was performed in non-total internal reflection configuration.

probe: BODIPY-G_{M1} appears to be incorporated stochastically into pre-existing platforms.

The mobility of BODIPY-G_{M1} was similar to that of mGFP-GPI ($D = 1.37 \pm 0.08\ \mu m^2/s$) (supplemental Fig. 6*D*). In particular, the same diffusion constant was obtained for BODIPY-G_{M1} irrespective of whether the experiment was performed in TOCCSL mode or at low surface density using conventional single molecule tracking (supplemental Fig. 6, compare *D* and *E*). Considering the size dependence of diffusion (34, 35), we conclude that both experiments addressed similar diffusing objects. This finding further confirms that pre-existing platforms were labeled by the lipid analog.

Platforms on Jurkat T Cells—Because rafts were particularly discussed as important structures in T cell signaling (38), we repeated the experiments on Jurkat T cells. For both mGFP-GPI and BODIPY-G_{M1}, we found clear cholesterol-dependent homo-association, similar to the results obtained with CHO cells (Fig. 2*B and* supplemental Fig. 4, *C* and *D*; data on diffusion constants can be found in supplemental Fig. 6, *F–I*).

When reducing the temperature to 25 °C, we observed a shift in the population toward larger structures, including up to 15% trimers and even tetramers, using again BODIPY-G_{M1} as a probe on Jurkat T cells (Fig. 3*A*). The relative fractions of the observed *n*-mers closely followed a Poisson distribution (Fig. 3*B*), as expected when the probe was randomly distributed over pre-existing platforms. A fit yielded the average number of fluorescent cargo molecules per platform (λ); note that this parameter also accounts for structures that by chance remained empty. *A priori*, however, it remained to be shown whether a subfraction of BODIPY-G_{M1} might also have partitioned into the bulk phase, where molecules would have moved as free monomers. We therefore tested also a generalized model that takes probe partitioning into the bulk phase into account. We reasoned that a potential non-raft fraction of BODIPY-G_{M1} would appear as additional monomers and that the resulting *n*-mer distribution would deviate from the Poisson model. However, fitting the distributions shown in Fig. 3*B* by Equation 1 yielded partition coefficients close to zero ($p = 0.1 \pm 0.1$), indicating that there is hardly any free BODIPY-G_{M1} in the non-raft fraction of the Jurkat T cell plasma membrane at 25 °C.

The platform loading (λ) was found to increase linearly with the probe density (σ) (Fig. 3*C*, *triangles*; see also supplemental Fig. 7*B*). From the reciprocal slope of the curve, we were able to estimate the surface density of platforms, $\zeta = \sigma/\lambda = 1300\ \mu m^{-2}$. For comparison, also data obtained at 37 °C with Jurkat T cells and CHO cells were included, assuming the Poisson model for platform loading. Also, linear increases were observed yet with reduced slope. Note that in the latter cases, BODIPY-G_{M1} partitioning into the bulk phase could not be excluded because analysis of the stoichiometric composition did not reveal cluster sizes (n) >2, rendering the calculation of a partition coefficient unfeasible. The reduction at 37 °C thus may either indicate a higher surface density of platforms (ζ) or may also be the consequence of BODIPY-G_{M1} leakage into the bulk phase.

Mild Fever-type Heat Shock Releases mGFP-GPI Homo-association—There is a long history of speculations for the involvement of lipid rafts in cell signaling (1). However, up to now, hardly any report has been available providing a direct link between raft properties and signal initiation. As a first field of application of our new technology, we attempted to test whether a rather general signaling mechanism, the expression of heat shock proteins upon mild heat stress, is correlated with a structural change in the plasma membrane. The rich phase behavior observed in binary or ternary model membranes (39) rendered the assumption of a temperature-induced switch in the formation of plasma membrane domains attractive. Indeed, mild fever-type heat shock response was speculated to be initiated by membrane raft reorganization (40, 41); a recent report showed that mild heating is

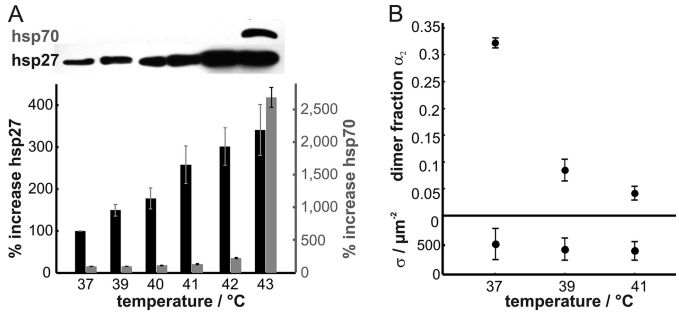

FIGURE 4. **Effect of temperature on the expression of heat shock proteins and the homo-association of mGFP-GPI.** *A*, CHO cells stably expressing mGFP-GPI were subjected to heat at the indicated temperatures or left at 37 °C for 60 min. After a 16-h recovery at 37 °C, the expression levels of Hsp27 and Hsp70 were determined by Western blotting. Whereas Hsp70 expression remained at basal levels at mild heat stress, Hsp27 expression showed already a considerable increase at 39 °C. *B*, TOCCSL experiments were performed on the same cells at the indicated temperatures. The dimer fraction (α_2) was found to decline substantially when increasing the temperature (*top*). The mean surface density of mGFP-GPI did not change with temperature (*bottom*).

sensed in the plasma membrane of plants cells (42). Up to now, however, there has been no direct experimental evidence for the influence of temperature on raft properties. For the following experiment, we reverted to our CHO cell line overexpressing mGFP-GPI. Consistent with previous reports (40, 43), we found differential heat shock response of small and large heat shock proteins: upon exposing the cells to mild heat shock of 39–42 °C, we observed elevated levels of the small heat shock protein Hsp27, whereas the expression of the large heat shock protein Hsp70 remained at basal levels (Fig. 4*A*). In the TOCCSL experiment, already a mild heat shock (39 °C) led to the almost total disappearance of mGFP-GPI homo-association, which became even more pronounced at 41 °C (Fig. 4*B*). This is a switch of remarkable steepness, centered exactly at the transition from physiological to fever-type temperatures. It is thus attractive to speculate that the plasma membrane may be involved in sensing small temperature elevations. Interestingly, in artificial bilayer systems, atomic force microscopy studies have shown that GPI-anchored proteins can be released from the liquid-ordered phase by an increase in temperature (44); a similar mechanism may account for the observed dissociation of mGFP-GPI homo-associates in the CHO cell membrane.

DISCUSSION

We have shown that the live cell plasma membrane contains, even in its resting state, mobile long-lived platforms hosting GPI-anchored proteins and glycolipids. Direct imaging of these structures became feasible with a new single molecule microscopy approach in combination with a specific photobleaching protocol. The observed structures show features reminiscent of lipid rafts (5). (i) The homo-association of the GPI-anchored protein and the liquid-ordered phase lipid BODIPY-G_{M1} depends on plasma membrane cholesterol levels, indicating that cohesion is mediated by the lipid environment. (ii) The observed BODIPY-G_{M1} platforms are of nanometer size. An upper limit can be given by the average distance between neighboring platforms ($\zeta^{-0.5}$); for Jurkat T cells at 25 °C, we found $\zeta = 1300$ μm^{-2}, yielding $\zeta^{-0.5} \sim 28$ nm.

For 37 °C, the low cargo load per platform prevented the test for Poisson loading distribution; thus, we cannot exclude the presence of free BODIPY-G_{M1} monomers in the plasma membrane. Still, the average distance between the nearest dimers observed at the maximum label density provides a conservative upper limit of the platform size, yielding ~45 nm for experiments on Jurkat and CHO cells. Assuming the validity of the Poisson model, we estimate $\zeta^{-0.5} \sim 18$ nm.

Together, our data reveal a new view on the nanoscopic landscape of the plasma membrane: there are lipids and lipid-anchored proteins, which diffuse as integral parts of long-lived platforms. Because mGFP-GPI partitions into detergent-resistant membranes and because probe association was found to be sensitive to cholesterol, the observed platforms can be related to biochemically defined rafts. In particular, we found no cargo exchange between different entities, indicating an extremely stable assembly of the nanostructures. The cholesterol sensitivity shows that a specific lipid nanoenvironment is required; at this stage, however, we cannot rule out that also protein moieties contribute to the interaction and by this further stabilize the observed platforms.

Not only does our method allow for confirming the existence of long-lived membrane platforms, it further provides previously unavailable information (see also the supplemental material for a discussion of our data in relation to the recent literature). First, the TOCCSL approach allows the detection of mobile platforms and is therefore complementary to alternative technologies for studying immobile plasma membrane nanostructures via advanced fluorescence correlation spectroscopy (17, 18), single molecule tracking (45–48), or homo-FRET analysis in combination with photobleaching (16), which sense static heterogeneities of probe mobility or proximity. Note that both fluorescence correlation spectroscopy and single molecule tracking rely on the observation of mobile objects; however, information is sought on immobile structures that modulate the motion of the mobile objects. Second, our method is capable of identifying comparably long-lasting interactions with a lifetime of seconds, thereby extending the time window for analysis of molecular association in live cells by 2–3 orders of magnitude (49). Our observation of long-lived rafts contrasts with recently published hypotheses that abandoned the assumption of long-lived lipid platforms in favor of short-lived structures (4, 5); up to now, however, there was no experimental evidence supporting either of the two viewpoints. Third, TOCCSL is a method for direct imaging of individual platforms. It is therefore suitable for combination with other fluorescence microscopy tools such as multicolor detection for colocalization studies or FRET analysis for assaying raft size and substructures.

The new approach opens up the perspective of going beyond applications on resting cells toward a functional raft investigation. With the capability to study nanostructures under physiological conditions, the functional consequence of a trigger (for example, the change in temperature or other environmental conditions or the application of external ligands) can now be linked to a structural modification in the plasma membrane.

Acknowledgments—We thank Jennifer Lippincott-Schwartz for providing pJB20/GFP-GPI, Christoph Metzner for providing purified His-mGFP-GPI(CD55), and Ken Jacobson for thoughtful discussions.

REFERENCES

1. Simons, K., and Toomre, D. (2000) *Nat. Rev. Mol. Cell Biol.* **1,** 31–39
2. Lingwood, D., and Simons, K. (2010) *Science* **327,** 46–50
3. Simons, K., and Ikonen, E. (1997) *Nature* **387,** 569–572
4. Kusumi, A., Koyama-Honda, I., and Suzuki, K. (2004) *Traffic* **5,** 213–230
5. Pike, L. J. (2006) *J. Lipid Res.* **47,** 1597–1598
6. Brown, D. A., and Rose, J. K. (1992) *Cell* **68,** 533–544
7. von Haller, P. D., Donohoe, S., Goodlett, D. R., Aebersold, R., and Watts, J. D. (2001) *Proteomics* **1,** 1010–1021
8. Foster, L. J., De Hoog, C. L., and Mann, M. (2003) *Proc. Natl. Acad. Sci. U.S.A.* **100,** 5813–5818
9. Stefanová, I., Horejsí, V., Ansotegui, I. J., Knapp, W., and Stockinger, H. (1991) *Science* **254,** 1016–1019
10. Dietrich, C., Volovyk, Z. N., Levi, M., Thompson, N. L., and Jacobson, K. (2001) *Proc. Natl. Acad. Sci. U.S.A.* **98,** 10642–10647
11. Schroeder, R., London, E., and Brown, D. (1994) *Proc. Natl. Acad. Sci. U.S.A.* **91,** 12130–12134
12. Heerklotz, H. (2002) *Biophys. J.* **83,** 2693–2701
13. Harder, T., Scheiffele, P., Verkade, P., and Simons, K. (1998) *J. Cell Biol.* **141,** 929–942
14. Sharma, P., Varma, R., Sarasij, R. C., Ira, Gousset, K., Krishnamoorthy, G., Rao, M., and Mayor, S. (2004) *Cell* **116,** 577–589
15. Varma, R., and Mayor, S. (1998) *Nature* **394,** 798–801
16. Goswami, D., Gowrishankar, K., Bilgrami, S., Ghosh, S., Raghupathy, R., Chadda, R., Vishwakarma, R., Rao, M., and Mayor, S. (2008) *Cell* **135,** 1085–1097
17. Lenne, P. F., Wawrezinieck, L., Conchonaud, F., Wurtz, O., Boned, A., Guo, X. J., Rigneault, H., He, H. T., and Marguet, D. (2006) *EMBO J.* **25,** 3245–3256
18. Eggeling, C., Ringemann, C., Medda, R., Schwarzmann, G., Sandhoff, K., Polyakova, S., Belov, V. N., Hein, B., von Middendorff, C., Schönle, A., and Hell, S. W. (2009) *Nature* **457,** 1159–1162
19. Shaw, A. S. (2006) *Nat. Immunol.* **7,** 1139–1142
20. Munro, S. (2003) *Cell* **115,** 377–388
21. Moertelmaier, M., Brameshuber, M., Linimeier, M., Schütz, G. J., and Stockinger, H. (2005) *Appl. Phys. Lett.* **87,** 263903
22. Ruprecht, V., Brameshuber, M., and Schütz, G. J. (2010) *Soft Matter* **6,** 568–581
23. Sengupta, P., Hammond, A., Holowka, D., and Baird, B. (2008) *Biochim. Biophys. Acta* **1778,** 20–32
24. Muhammad, A., Schiller, H. B., Forster, F., Eckerstorfer, P., Geyeregger, R., Leksa, V., Zlabinger, G. J., Sibilia, M., Sonnleitner, A., Paster, W., and Stockinger, H. (2009) *J. Immunol.* **182,** 7672–7680
25. Gombos, I., Bacsó, Z., Detre, C., Nagy, H., Goda, K., Andrásfalvy, M., Szabó, G., and Matkó, J. (2004) *Cytometry A.* **61,** 117–126
26. Janes, P. W., Ley, S. C., and Magee, A. I. (1999) *J. Cell Biol.* **147,** 447–461
27. Yancey, P. G., Rodrigueza, W. V., Kilsdonk, E. P., Stoudt, G. W., Johnson, W. J., Phillips, M. C., and Rothblat, G. H. (1996) *J. Biol. Chem.* **271,** 16026–16034
28. Metzner, C., Mostegl, M. M., Günzburg, W. H., Salmons, B., and Dangerfield, J. A. (2008) *FASEB J.* **22,** 2734–2739
29. Ruprecht, V., Brameshuber, M., and Schutz, G. J. (2010) *Soft Matter* **6,** 568–581
30. Wieser, S., and Schütz, G. J. (2008) *Methods* **46,** 131–140
31. Schmidt, T., Schütz, G. J., Gruber, H. J., and Schindler, H. (1996) *Anal. Chem.* **68,** 4397–4401
32. Paladino, S., Lebreton, S., Tivodar, S., Campana, V., Tempre, R., and Zurzolo, C. (2008) *J. Cell Sci.* **121,** 4001–4007
33. Kenworthy, A. K., Nichols, B. J., Remmert, C. L., Hendrix, G. M., Kumar, M., Zimmerberg, J., and Lippincott-Schwartz, J. (2004) *J. Cell Biol.* **165,** 735–746
34. Saffman, P. G., and Delbrück, M. (1975) *Proc. Natl. Acad. Sci. U.S.A.* **72,** 3111–3113
35. Gambin, Y., Lopez-Esparza, R., Reffay, M., Sierecki, E., Gov, N. S., Genest, M., Hodges, R. S., and Urbach, W. (2006) *Proc. Natl. Acad. Sci. U.S.A.* **103,** 2098–2102
36. Lebreton, S., Paladino, S., and Zurzolo, C. (2008) *J. Biol. Chem.* **283,** 29545–29553
37. Kwik, J., Boyle, S., Fooksman, D., Margolis, L., Sheetz, M. P., and Edidin, M. (2003) *Proc. Natl. Acad. Sci. U.S.A.* **100,** 13964–13969
38. Harder, T., Rentero, C., Zech, T., and Gaus, K. (2007) *Curr. Opin. Immunol.* **19,** 470–475
39. Veatch, S. L., and Keller, S. L. (2005) *Biochim. Biophys. Acta* **1746,** 172–185
40. Nagy, E., Balogi, Z., Gombos, I., Akerfelt, M., Björkbom, A., Balogh, G., Török, Z., Maslyanko, A., Fiszer-Kierzkowska, A., Lisowska, K., Slotte, P. J., Sistonen, L., Horváth, I., and Vígh, L. (2007) *Proc. Natl. Acad. Sci. U.S.A.* **104,** 7945–7950
41. Vigh, L., Escribá, P. V., Sonnleitner, A., Sonnleitner, M., Piotto, S., Maresca, B., Horváth, I., and Harwood, J. L. (2005) *Prog. Lipid Res.* **44,** 303–344
42. Saidi, Y., Finka, A., Muriset, M., Bromberg, Z., Weiss, Y. G., Maathuis, F. J., and Goloubinoff, P. (2009) *Plant Cell* **21,** 2829–2843
43. Krishnan, J., Lemmens, R., Robberecht, W., and Van Den Bosch, L. (2006) *Exp. Neurol.* **200,** 301–310
44. Giocondi, M. C., Besson, F., Dosset, P., Milhiet, P. E., and Le Grimellec, C. (2007) *J. Mol. Recognit.* **20,** 531–537
45. Sergé, A., Bertaux, N., Rigneault, H., and Marguet, D. (2008) *Nat. Methods* **5,** 687–694
46. Manley, S., Gillette, J. M., Patterson, G. H., Shroff, H., Hess, H. F., Betzig, E., and Lippincott-Schwartz, J. (2008) *Nat. Methods* **5,** 155–157
47. Hess, S. T., Gould, T. J., Gudheti, M. V., Maas, S. A., Mills, K. D., and Zimmerberg, J. (2007) *Proc. Natl. Acad. Sci. U.S.A.* **104,** 17370–17375
48. Douglass, A. D., and Vale, R. D. (2005) *Cell* **121,** 937–950
49. Haustein, E., and Schwille, P. (2007) *Annu. Rev. Biophys. Biomol. Struct.* **36,** 151–169